Journal of Rock Mechanics and Geotechnical Engineering 11 (2019) 920–934

Contents lists available at ScienceDirect

Journal of Rock Mechanics and Geotechnical Engineering

journal homepage: www.rockgeotech.org

Full Length Article

Evaluation of earthquake impact on magnitude of the minimum principal stress along a shotcrete lined pressure tunnel in Nepal

Krishna Kanta Panthi*, Chhatra Bahadur Basnet

Department of Geoscience and Petroleum, Norwegian University of Science and Technology, Trondheim 7491, Norway

ARTICLE INFO

Article history:
Received 25 October 2018
Received in revised form
29 March 2019
Accepted 12 June 2019
Available online 30 July 2019

Keywords:
Shotcrete lined pressure tunnel
The minimum principal stress
Three-dimensional (3D) numerical model
Geology
Tectonic activity
Himalaya

ABSTRACT

In situ stress condition in rock mass is influenced by both tectonic activity and geological environment such as faulting and shearing in the rock mass. This influence is of significance in the Himalayan region, where the tectonic movement is active, resulting in periodic dynamic earthquakes. Each large-scale earthquake causes both accumulation and sudden release of strain energy, instigating changes in the in situ stress environment in the rock mass. This paper first highlights the importance of the magnitude of the minimum principal stress in the design of unlined or shotcrete lined pressure tunnel as water conveyance system used for hydropower schemes. Then we evaluated the influence of local shear faults on the magnitude of the minimum principal stress along the shotcrete lined high pressure tunnel of Upper Tamakoshi Hydroelectric Project (UTHP) in Nepal. A detailed assessment of the in situ stress state is carried out using both measured data and three-dimensional (3D) numerical analyses with FLAC^{3D}. Finally, analysis is carried out on the possible changes in the magnitude of the minimum principal stress in the rock mass caused by seismic movement (dynamic loading). A permanent change in the stress state at and nearby the area of shear zones along the tunnel alignment is found to be an eminent process.

1. Introduction

Unlined pressure tunnels and shafts are used in the hydropower projects worldwide. Especially in Norway, more than 95% of the total hydropower tunnels and shafts are unlined. Such tunnels and shafts in Norway are considered to be possible due to the favorable engineering geological and geotectonic conditions in this region (Buen, 1984; Panthi, 2014). During the process of design, construction and operation of such tunnels, Norway has gradually developed different design criteria over the time (Selmer-Olsen, 1969; Bergh-Christensen, 1982; Broch, 1982; Buen and Palmstrom, 1982). The state-of-the-art criterion is that the in situ minimum principal stress should be higher than the static water pressure acting on the periphery of unlined or shotcretre lined pressure tunnels and shafts (Selmer-Olsen, 1974; Broch, 1982; Panthi, 2014). This condition of in situ stress is required in order to avoid possible hydraulic jacking. Correct evaluation of the in situ minimum principal stress is therefore the key for the successful design of unlined or shotcrete lined high pressure tunnels and shafts.

In the Himalaya, a shotcrete lined pressure tunnel is being implemented at the headrace tunnel system of the Upper Tamakoshi Hydroelectric Project (UTHP) in Nepal. Panthi and Basnet (2017) highlighted that one of the design issues in this shotcrete lined tunnel is the magnitude of the minimum principal stress. At UTHP, in situ stresses were initially measured using three-dimensional (3D) overcoring method inside the test tunnel excavated at the bottom of Tamakoshi River valley (SINTEF, 2008). Based on the measured stress state, the location of the headrace tunnel was selected in such a way that the maximum internal water pressure became about 4.2 MPa (420 m water head) at the end of the headrace tunnel. This decision was based on the assumption that the in situ stress state along the headrace tunnel alignment will be similar to that of the stress measurement location. However, the minimum principal stress measured by hydraulic fracturing (SINTEF, 2013) at the end of the headrace tunnel indicated that the available minimum principal stress is not sufficient to avoid the potential hydraulic jacking and leakage through the headrace tunnel. As a result, the tunnel alignment was shifted to a new location at the upper elevation, where outer part of the shotcrete lined headrace tunnel will now experience a maximum pressure of about 1.15 MPa (115 m water head).

* Corresponding author.
E-mail address: krishna.panthi@ntnu.no (K.K. Panthi).
Peer review under responsibility of Institute of Rock and Soil Mechanics, Chinese Academy of Sciences.

https://doi.org/10.1016/j.jrmge.2019.06.003

It is highlighted that the ground conditions along the shotcrete lined pressure tunnel at the UTHP were assumed to be competent and thought to be as similar as that of the Norwegian hydropower projects where unlined pressure tunnels and shafts are very common solutions. However, according to McGarr and Gay (1978) and Panthi (2014), the total stress field at a particular region is influenced by the geological history as well as tectonic and gravitational forces, which are unique themselves. It is highlighted here that one of the reasons for the success of unlined high pressure tunnel and shaft concept in Norway is that the region is hard rock domain, relatively stable regarding tectonic activity and deglaciation effect. The Himalayan region, on the other hand, is tectonically active where medium- to large-scale earthquakes are very common. Therefore, in addition to static stress analysis, a dynamic stress analysis has to be carried out to estimate the magnitude of the minimum principal stress, which can be used as an input in the design of unlined/shotcrerte lined pressure tunnels, which is normally not important in Norway.

In light of the above background, the main aim of this article is to evaluate the in situ stress state of the Tamakoshi area with due consideration of both static and dynamic (earthquake) loadings. In this regard, a 3D numerical model established by FLAC^{3D} is exploited to overcome the limitation of two-dimensional (2D) assessments. In addition, the 3D model gives possibility to incorporate complex topography and geological defects like weakness and shear zones in the model. The model extent is chosen in such a way that the 3D geometry is generated within the FLAC^{3D} model so that both static and dynamic analyses can be carried out. Firstly, field measured in situ principal stresses are used to validate the model under static condition. Secondly, one of the recent earthquake aftershock (M_w = 7.3) on 12 May 2015, which had an epicenter nearby the project area and is also a major aftershock after the Gorkha earthquake mainshock (M_w = 7.8) on 25 April 2015, is considered in the dynamic analysis. Peak ground acceleration (PGA) of the aftershock at the project area computed by USGS (2015) is used to validate the model for dynamic analysis. Finally, the differences between the magnitudes of the minimum principal stresses from these two analyses at different locations along the headrace tunnel alignment are recorded so that any permanent changes in the magnitude of the minimum principal stresses along the headrace tunnel alignment could be identified.

2. Upper Tamakoshi project area

The UTHP is located in Dolakha District of Nepal, which is northeast from Kathmandu valley (Fig. 1). The project is under construction and has an installed capacity of 456 MW. To generate this installed capacity, the project exploits 66 m^3/s design discharge and 822 m gross head (Reimer and Bock, 2013). The project consists of different civil structures such as headworks, headrace tunnel, vertical penstock shafts, underground power station, and tailrace and access tunnels. In this paper, the main focus is given to the headrace tunnel system, which is designed as unlined or shotcrete lined pressure tunnel. There have been several changes in the design of headrace tunnel alignments at this project. In 2008, the headrace tunnel was designed to have a maximum static water head of about 420 m (4.2 MPa), which is represented as 'OLD HRT' in this paper. Later during excavation, it was realized that the rock mass is not suitable for the implementation of shotcrete lined tunnel for 420 m water pressure based on the minimum principal stress measured by hydraulic fracturing that gave considerably lower magnitude of the stresses than static water pressure. As a result, the headrace tunnel alignment was shifted upwards and also part of the tunnel was moved more towards the hill side (Fig. 2). The maximum static water head in this new alignment is now limited to about 115 m (1.15 MPa), which is denoted as 'NEW HRT' in this paper. It is emphasized here that the magnitudes of the minimum principal stresses along both old and new alignments have been the matter

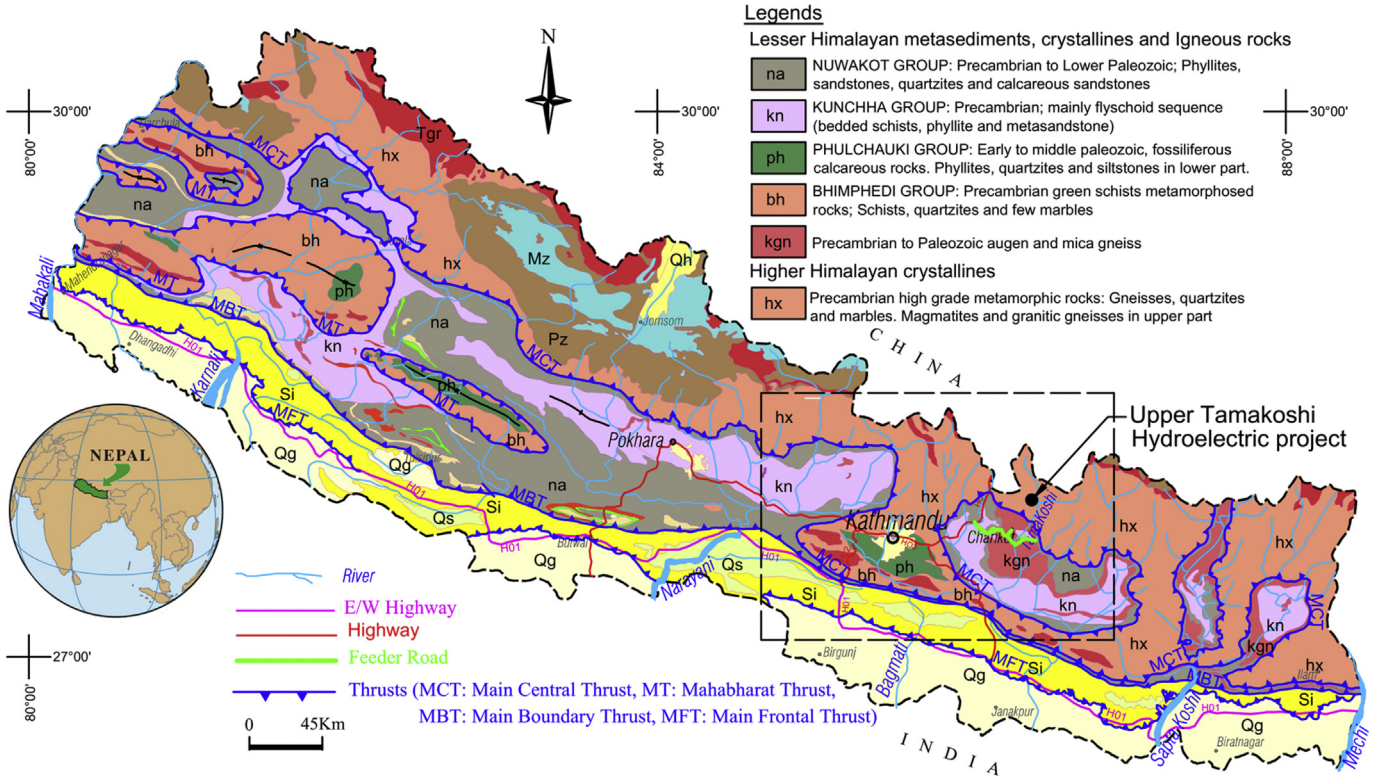

Fig. 1. Location of Upper Tamakoshi hydroelectric project in the geological map of Nepal.

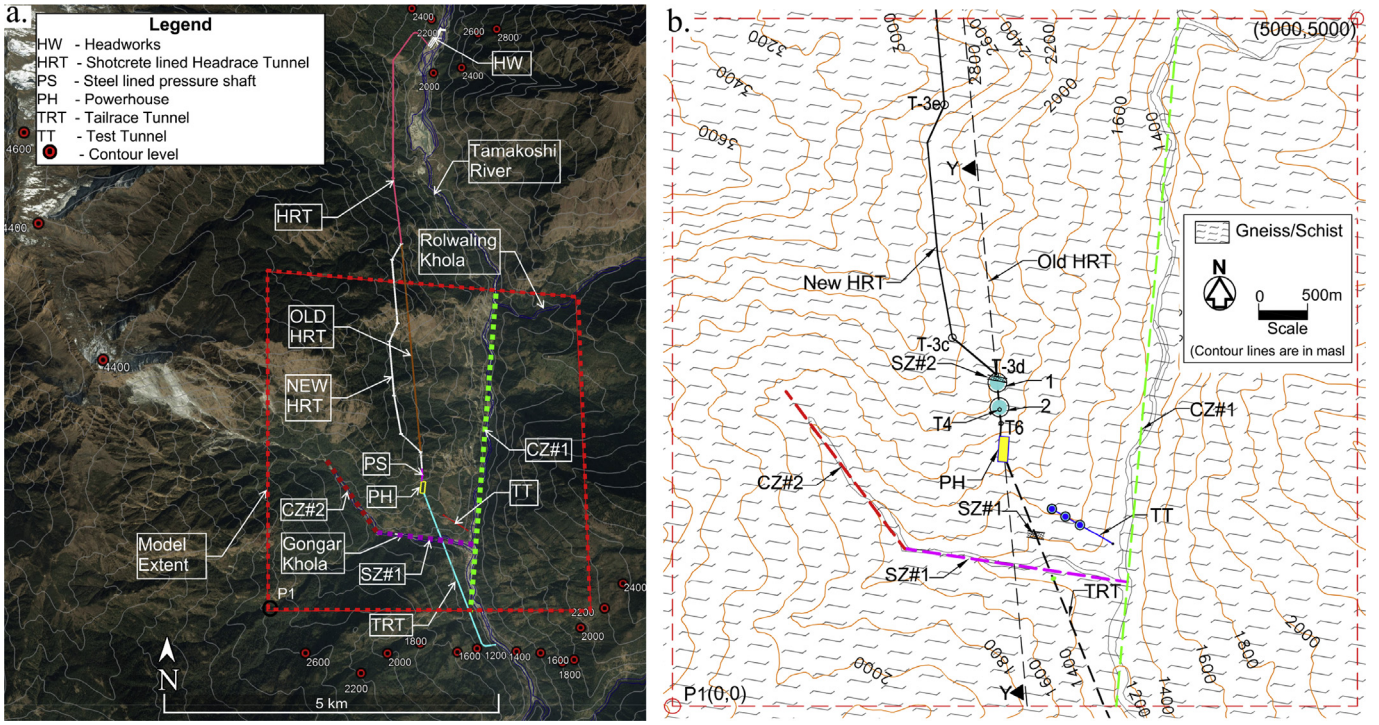

Fig. 2. (a) 3D topography, major lineaments and layout of Upper Tamakoshi project overlaid in Google Earth map; and (b) Topographic map of the project area included in model extent.

of great concern for the applicability of shotcrete lined tunnel at the UTHP. In general, the geology and tectonics of the Himalaya, topography, presence of influential weakness and shear zones, recent major earthquake activities surrounding the project area, and information about the magnitude and orientation of the tectonic stress in the vicinity are important information to be understood and considered for the overall stress state analysis considering both static and dynamic approaches.

2.1. Geology and tectonics

Geologically, the project is located in the Higher Himalayan Tectonic Formation of eastern Nepal Himalaya, as shown in Fig. 1 (Panthi and Basnet, 2017). Rock mass in this formation is mainly characterized by Precambrian high grade metamorphic rocks such as gneiss, quartzite, marbles, magmatite and granitic gneiss having the quality of rock mass comparable to the Scandinavian hard rock mass. In particular, the main rock type at the project area is mainly composed of micaceous schist and banded gneiss with abundant mica contents, which is commonly known as schistose gneiss (Norconsult, 2005). The rock mass of this area has three distinct joint sets including foliation joints. The general strikes of the foliation joints are WSW to WNW with dip angles of 35°–75°NW to NE.

Tectonically, the Himalaya region is very dynamic. A collision between the Indian and the Euro-Asian continental plates took place about 70–100 Ma ago, and as a result, the Himalaya was evolved. After the collision occurred, the Indian plate from the south is continuously under-thrusting to the upper crust of the Euro-Asian plate to date. Due to this fact, this region is being undergoing persistent compression and the rate of convergence is estimated to be about 5 cm/a (Bird, 1978; Nakata et al., 1990). Considerable amount of energy is being accumulated through this compressional process and the accumulated energy is being released through the rupture of tectonic faults and fractures causing periodic earthquakes. As a result, the magnitude of tectonic stress varies over the time due to sudden release and accumulation of the strain energy along the prevailing tectonic faults. The annual rate of long-term tectonic stress change induced by the subduction process is estimated to be in the order of some kPa (Panthi, 2006). The compressional tectonic deformation and active reverse faulting mechanism have considerable influence on the magnitude of rock stresses in the Himalaya. The general trend of the tectonic stress orientation in the Himalaya is NE–SW at the northwestern part of the Himalaya and is more or less N–S at the southeastern part (Panthi, 2012). The trend nearby the project area appears to be in the direction of approximately N20°–40°E.

2.2. Topography and weakness zones

The headrace tunnel is located along the right bank of the Tamakoshi River (Fig. 2). The highest elevation of the nearest hill from the headrace tunnel is about 4500 m above sea level (masl) and the lowest elevation is at the Tamakoshi River at about 1250 masl. The level difference is about 3300 m within a horizontal distance of about 5500 m and the slope of the terrain varies between 30° and 40°. The slope and the level difference show that the Tamakoshi River is a deep valley and the topography represents a high relief. In addition to the Tamakoshi River, there is Gongar Khola (a small river) near the outer reach of the headrace tunnel. The Gongar Khola is also a deep valley connected to the Tamakoshi valley making a confluence at an elevation of about 1250 masl. Both valleys will have to be considered in the stress state analysis for the logical estimation of the stress state of the project area.

The Tamakoshi River is inferred as a crushed zone and indicated as CZ#1 (Fig. 2). Similarly, the upper left tributary of the Gongar valley is also inferred as a crushed zone and is denoted as CZ#2. This zone is orienting away from the foliation of the rock mass and

the formation of the zone is assumed by the similar way as that of the CZ#1. In addition, four more weakness zones were encountered during tunnel excavation in the tailrace tunnel, the old headrace tunnel alignment (OLD HRT) and the new headrace tunnel alignment (NEW HRT), which were considered as shear zones and denoted as SZ#1, SZ#2, SZ#3 and SZ#4 (Figs. 2b and 3a), respectively. The orientations of these zones are along the foliation of the rock mass (Fig. 3b).

2.3. Measured stress at UTHP

At UTHP, both 3D overcoring and hydraulic fracturing techniques were used to measure the in situ stress state at different locations, as shown in Fig. 4. The measurements were carried out at two different elevation levels of the topography at different project development stages.

2.3.1. 3D overcoring

In 2008, at about bottom valley level nearby the Gongar and Tamakoshi valleys, 3D stresses were measured at locations TT1, TT2 and TT3 in test tunnel (TT) by using 3D overcoring technique (SINTEF, 2008). The test detail was given in the report of SINTEF (2008). In summary, the overcoring process started with diamond drilling of a core hole of 76 mm in outer diameter to a desired length. The bottom of the hole was flattened and a concentric hole with 36 mm diameter was subsequently drilled 30 cm further. A measuring cell consisting of strain gages was inserted into the small hole and initial reading was done (0 reading in strain gages). The small hole containing the measuring cell was then overcored by a larger drill bit so that the stresses were relieved in the core and the corresponding strains were recorded. Finally, the core was extracted from the drill hole by a dedicated core catcher and immediately after removal from the hole, the second reading was taken. The same process was repeated for all measurement locations. The test location details are shown in Fig. 5.

The computer program called DISO (determination of in situ stress by overcoring) developed by SINTEF was used to calculate the magnitude and orientation of principal stresses from the strain readings and laboratory tested elastic parameters consisting of Young's modulus and Poisson's ratio of rock using the rock cores collected from the corresponding measurement locations. The DISO program computes the in situ stresses by randomly selecting the strain readings from the measurements. The program automatically removes obvious erroneous strain values and further performs statistical calculations resulting in mean values of the principal stresses and respective standard deviation (SD) (Lu, 2006). The mean values of principal stresses with respective SDs and orientation of corresponding stresses are given in Table 1.

2.3.2. Hydraulic fracturing

After about 265 m excavation of the OLD HRT from downstream end, a shear zone was encountered (SZ#2 in Fig. 3a). With further headrace tunnel excavation of about 200 m (up to point *EE* in Fig. 3a), it was realized that the rock mass at the downstream end of the headrace tunnel is destressed. Following the design phase recommendation, hydraulic fracturing test was carried out to verify suitability for the implementation of shotcrete lined pressure tunnel from this elevation, which gave a static water head of 420 m (4.2 MPa). The magnitude of the minimum principal stress was measured by SINTEF (2013) at locations 1 and 2 along the excavated tunnel (the locations are shown in Fig. 4 and the test location details are shown in Fig. 6). The measurement procedure of the hydraulic fracturing tests and the determination of the results follow the standards suggested by the International Society for Rock Mechanics and Rock Engineering (ISRM) (Haimson and Cornet, 2003) excluding that the fracture orientation was not determined since the purpose of the test was just to measure the magnitude of the minimum principal stress. The measurement details and test results were explained in detail in the report by SINTEF (2013). The hydraulic fracturing test equipment was placed at a desired borehole depth and two packers were inflated with water, closing a borehole section of about 1 m. Each test section included initial fracturing of intact rock, which meant inducing a new fracture in the rock mass. The water pressure required to induce this initial fracture is called fracturing pressure P_f. The test was then followed by re-openings of the induced fracture. The pressure required to re-open the fracture is called fracture re-opening pressure P_r. The applied water pressure, packer pressure, and water flow rate were continuously logged during the whole test. The shut-in pressure was identified as the point at which the flow is closing in the test section. In each test sections in the borehole, at least three test cycles were conducted. Finally, the magnitude of the minimum principal stress was represented by the shut-in pressure P_{si} in each cycle. Altogether, 7 measurements at different depths of four boreholes at location 1 and 19 measurements at different depths of four boreholes at location 2 were successfully conducted (all test results are given in Table 2).

Once the magnitude of the minimum principal stress (S_3) is determined, the magnitude of the maximum principal stress (S_1) is calculated using the relationship given in Eq. (1) with known value

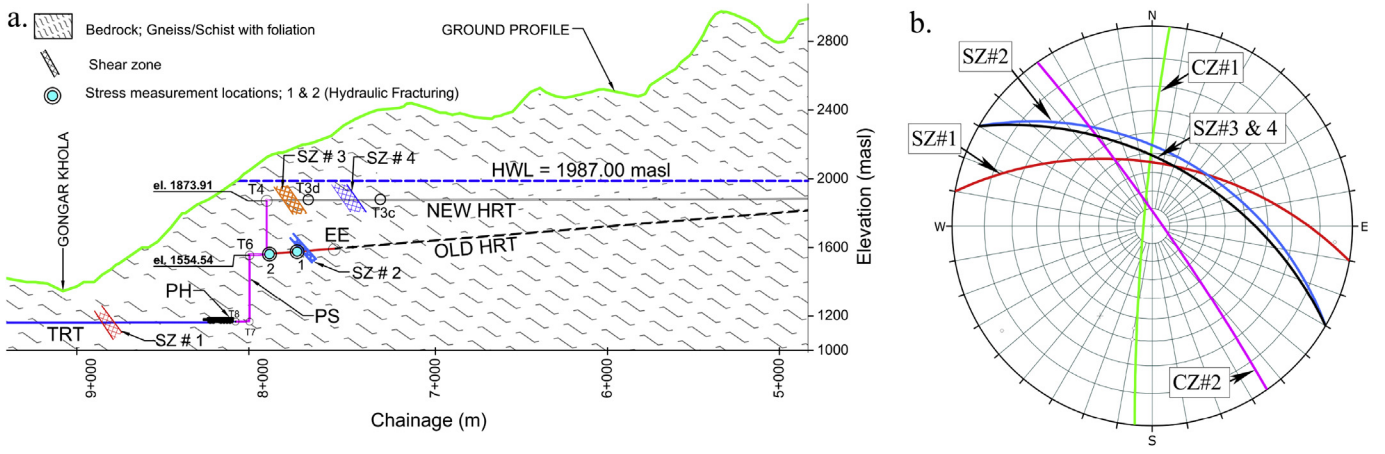

Fig. 3. (a) Tunnel alignment profile with geology ('HWL' is the highest water level); and (b) Stereographic projection of weakness zones (lower hemisphere, equal angle).

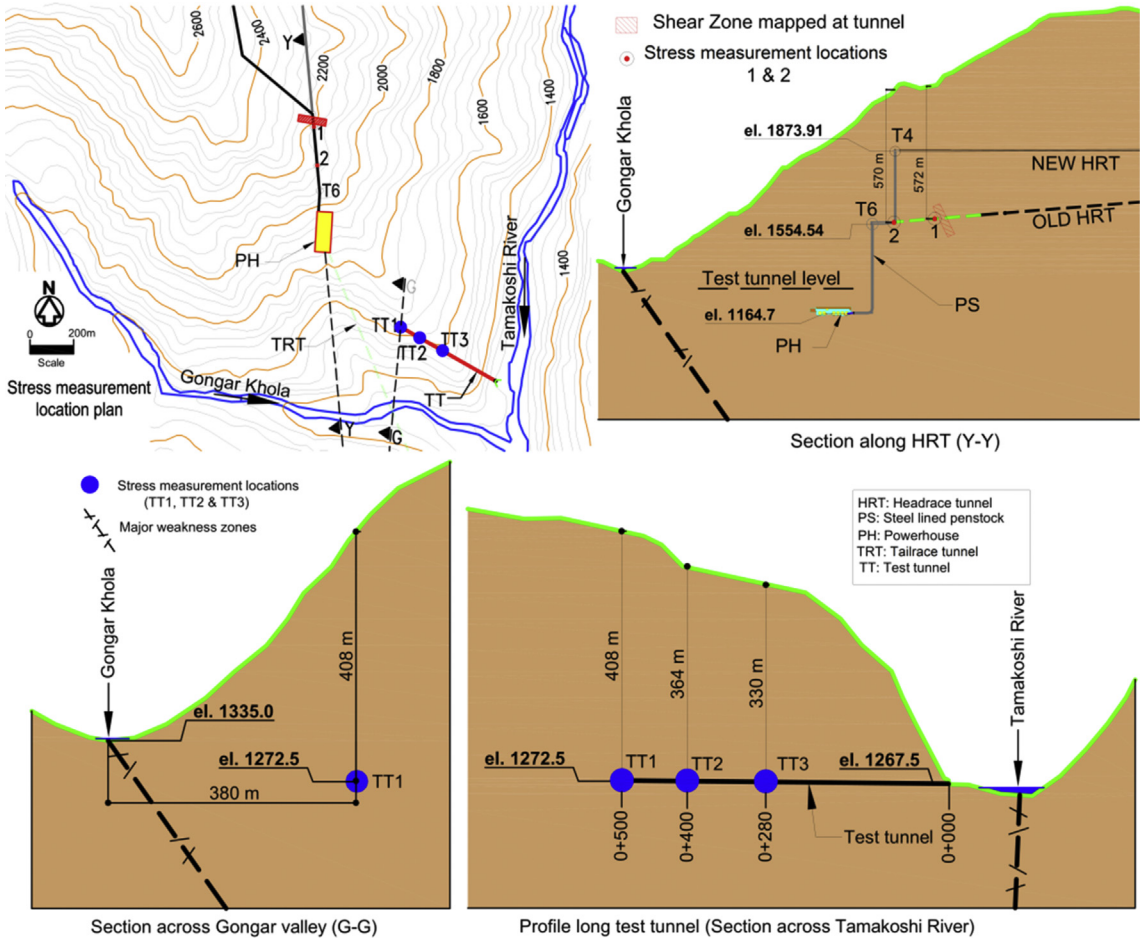

Fig. 4. Stress measurement locations TT1, TT2, TT3, 1 and 2 (all dimensions are in m).

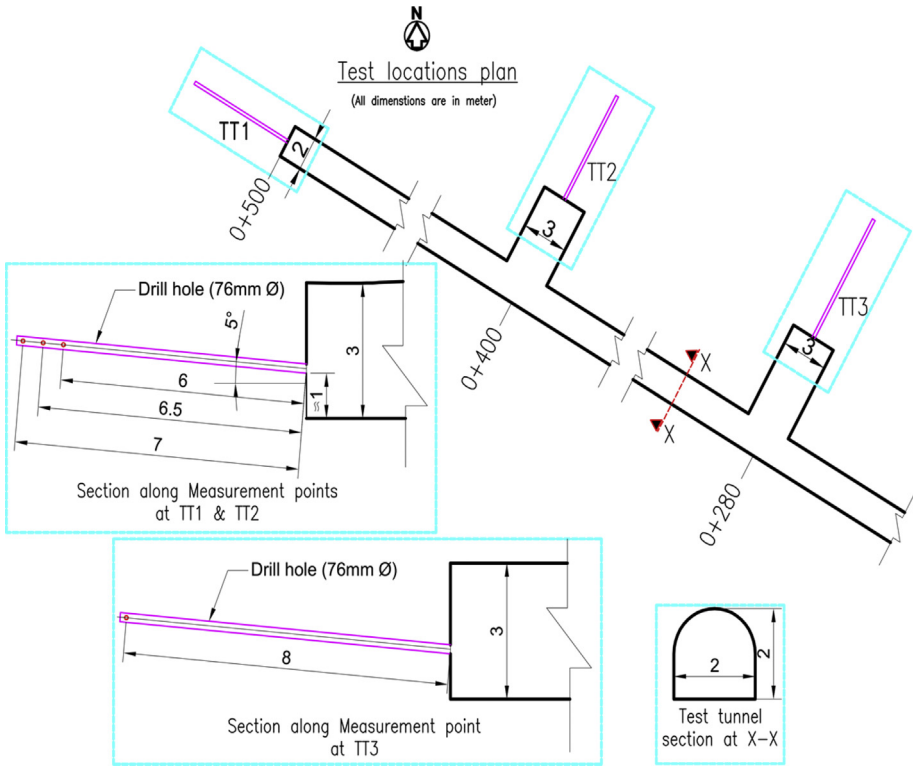

Fig. 5. Stress measurement details at locations TT1, TT2 and TT3 (all dimensions are in m).

Table 1
Final values of magnitude and orientation of the principal stresses at TT1, TT2 and TT3.

Location	Maximum principal stress, S_1			Intermediate principal stress, S_2			Minimum principal stress, S_3		
	Mean (MPa)	SD (MPa)	Orientation (°)	Mean (MPa)	SD (MPa)	Orientation (°)	Mean (MPa)	SD (MPa)	Orientation (°)
TT1	18.4	2.9	120/28	12.4	4.7	240/42	7.1	1.8	9/35
TT2	17.4	2.2	205/30	10.8	1.7	100/23	1.1	2.7	339/50
TT3	21.6	3.8	21/10	12.6	2.8	117/27	6.4	4.8	272/61

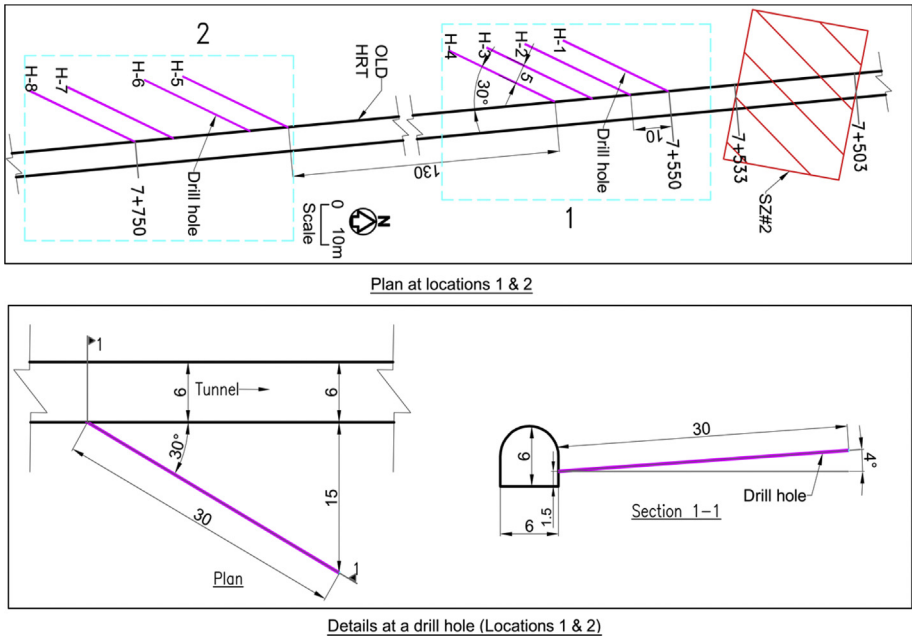

Fig. 6. Location plan details at locations 1 and 2 (all dimensions are in m).

of fracturing pressure (P_f) and tensile strength of the rock (S_t). In this regard, the fracturing pressure measured at different test locations (Table 2) and the tensile strength of the rock tested by the authors are used in the calculation. The tensile strength of the rock has been tested using Brazilian test procedure suggested by the ISRM (1978).

$$S_1 = 3S_3 - P_f + S_t \quad (1)$$

Eq. (1) is slightly modified from the original equation given by Haimson and Cornet (2003). Since the boreholes are sub-horizontal in both locations, the originally recommended relationship for vertical borehole is modified keeping in mind that the fracture is induced in the direction perpendicular to the minimum principal stress. Finally, Table 3 shows the statistical distribution of magnitude of both the the maximum and the minimum principal stresses based on hydraulic fracturing at both locations 1 and 2.

2.4. Recent earthquake activities nearby the UTHP

The whole Himalaya region is very dynamic and has been witnessing a large number of earthquakes of various magnitudes. More recently, an earthquake of a magnitude of $M_w = 7.8$ occurred on 25 April 2015 (Fig. 7). The epicenter of this event was at Barpak village of Gorkha District of Nepal and is famously known as Gorkha earthquake. Series of aftershocks of varying magnitudes occurred following this main event. As one can see in Fig. 7, numerous aftershocks of varying magnitudes ($M_w > 4$) occurred during the period from 25 April 2015 to date. As shown in the figure, one of the aftershocks occurred at NE-Kalinchowk of the Dolakha District of Nepal on 12 May 2015, which was the largest aftershock with a magnitude of $M_w = 7.3$. The UTHP is relatively close (about 13 km) to the epicenter of this aftershock (Fig. 7). The characteristic of the seismic waves of this aftershock was discussed by Bhattarai et al. (2015).

In this study, the authors attempted to simulate the seismic waves generated during the aftershock of $M_w = 7.3$, which was believed by the authors to have strong impact on the project area due to closeness. Simulation of real-time seismic wave generated during the earthquake is challenging due to varying frequencies and amplitudes over the seismic (dynamic) period. It is thus decided to use PGA as the amplitude of the seismic acceleration, which is supposed to be the most influential event of this episode regarding in situ stress changes in the project area. In this regard, the PGA computed by USGS (2015) in terms of a fraction of g (acceleration due to gravity) has been used. The PGA contours in and around the project area are shown in Fig. 8. The PGA values shown in Fig. 8 are computed from the characteristics of the seismic waves generated during the aftershock of $M_w = 7.3$. Fig. 8 indicates that the PGA value at the surface above the downstream end of the shotcrete lined pressure tunnel is about 0.4g.

3. Stress state analysis

Hart (2003) emphasized that it is important to identify the conditions that can influence the stress state before any assessment is made on the in situ stress conditions in an area of concern by numerical model. The conditions such as irregular surface

Table 2
Results from test locations 1 and 2 for each hole at different depths (SINTEF, 2013).

Location	Hole	Hole depth (m)	P_f (MPa)	P_r (MPa)	P_{si} (MPa)		
					1st cycle	2nd cycle	3rd cycle
1	H-1	27.5	*	–	–	–	–
		24.5	7.7	4.6	1.8	1.7	1.6
		21.5	*	–	–	–	–
		18.5	13*	11	3.5	3.7	3.7
		15.5	9.2	5.6	3.4	3.3	3.3
		12.5	9.8	5.4	3.4	3.5	3.5
	H-2	27.5	11	6.4	2.5	2.1	1.9
		24.5	*	–	–	–	–
		21.5	*	–	–	–	–
		15.5	*	–	–	–	–
	H-3	27	*	–	–	–	–
		24	*	–	–	–	–
		21	*	–	–	–	–
		18	*	–	–	–	–
		15	*	–	–	–	–
		12	*	–	–	–	–
	H-4	24	9.9	7.2	4.9	4.8	4.8
		21	8.6	7	3.4	3.5	3.5
		18	*	–	–	–	–
		15	*	–	–	–	–
2	H-5	28.6	*	–	–	–	–
		25.6	11.9	9.9	6.7	7.8	8
		22.6	*	–	–	–	–
		19.6	10	8.8	7.6	7.7	7.4
		16.6	13.5	11.1	7.6	7.7	8
		13.6	19.5	9.3	7.8	7.4	7.4
	H-6	28.5	10.5	6.7	5.1	5	5.3
		25.5	10.1	8.2	5.7	5.8	5.7
		22.5	19.1	15.5	8.9	8.7	8.9
		19.5	18.7	12.9	9.1	9.1	9.1
		16.5	12.1	10.5	8.9	9	9.1
		13.5	*	–	–	–	–
	H-7	27	12.5	–	1.8	–	–
		25.5	10.1	3.6	2.7	1.9	1.8
		24	6.4	4.3	2.5	2.3	1.9
		18	8.4	5.6	3.1	4	4.1
		21	*	–	–	–	–
		15	9.5	5.3	4.3	4.3	4.6
		12	10.8	3.7	1.4	1.2	1.5
	H-8	27	*	–	–	–	–
		24	11.1	5.7	3.9	3.8	3.8
		21	*	–	–	–	–
		18	10.8	5.1	4.5	4.4	4.4
		15	6.7	4.7	4.4	3.3	3.4
		12	7.2	6	3.9	4	3.9

Note: '*' stands for unsuccessful tests.

Table 3
Stress measurements by hydraulic fracturing at locations 1 and 2.

Location	S_3 (MPa)		S_t (MPa)		S_1 (MPa)	
	Mean	SD	Mean	SD	Mean	SD
1	3.2	1	10	1.2	10.1	3.2
2	5.4	2.5	10	1.2	14.2	6

topography, tectonic movement, stress perturbations due to faulting and localization and so forth can produce a complex in situ stress state even before excavation-induced stresses are imposed. Therefore, a complete stress estimation strategy, which includes all possible influential factors and the database of the stress state estimated using different techniques, should be adopted (Hudson et al., 2003). The authors further highlighted that complete stress information is necessary to compare the results from numerical analysis. In numerical analysis, the tectonic and gravitational stresses are the main stress inputs to the model. In addition, presence of discontinuity planes such as weakness and fault zones locally influences the in situ stress state by perturbing the stress

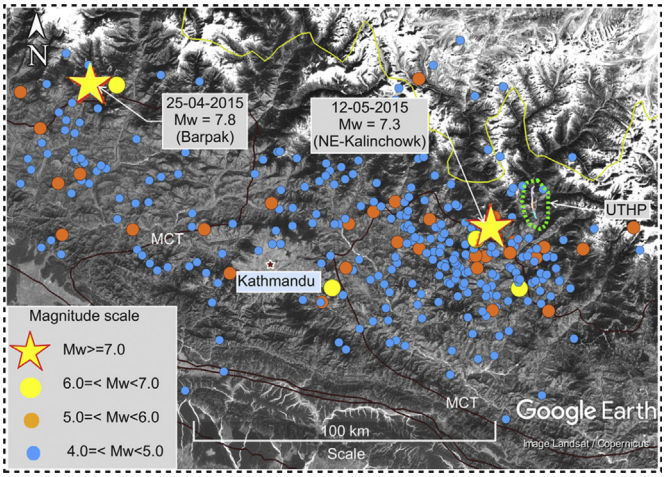

Fig. 7. Recorded earthquakes in and around the Upper Tamakoshi project area (inside the rectangle shown in Fig. 1) after the Gorkha earthquake in April 2015. Note that the main shock and major aftershock are shown with yellow stars and all other earthquakes are shown with filled circles, and the earthquake data are extracted from U.S. Geological Survey (https://earthquake.usgs.gov/earthquakes/map) and overlaid in Google Earth map.

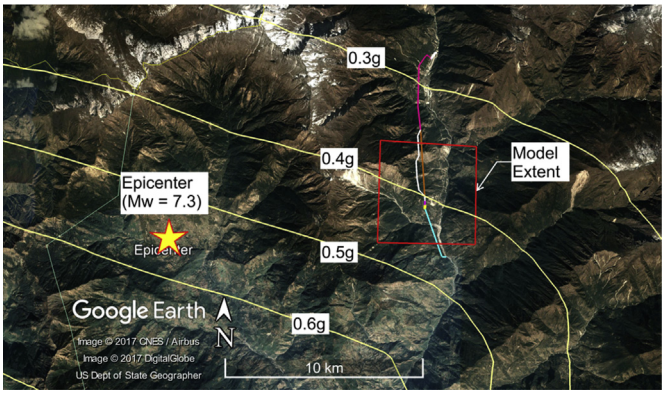

Fig. 8. Contours of peak ground acceleration as a fraction of g (source from KMZ file of USGS (2015) overlaid in Google Earth map).

trajectories. Numerical simulations can assist in indicating possible perturbations to the stress field caused by geological defects. Hence, numerical modeling using FLAC^{3D} (Itasca, 2017) is extensively used for the defined model extent of UTHP area in order to quantify the stress values at the location of interest. In this respect, both static and dynamic analyses are carried out. In static analysis, the measured stresses are used to validate the model and the minimum principal stresses are recorded at the tunnel locations. The statically validated model is further exploited for the dynamic loading in order to assess seismic influence on the stress state.

3.1. Modeling strategy

The modeling strategy adopted in this study is shown in Fig. 9. As one can see in the figure, the rock mechanical parameters are assigned in the model considering rock mass as isotropic and linearly elastic material. Boundaries at east, west, north, south and bottom faces are prevented for normal displacement to occur by fixing the corresponding velocities to zero values. In addition, the lateral boundaries are further prevented for horizontal tangential displacements in order to avoid stress concentration at the boundary corners, which is likely to occur due to the horizontal

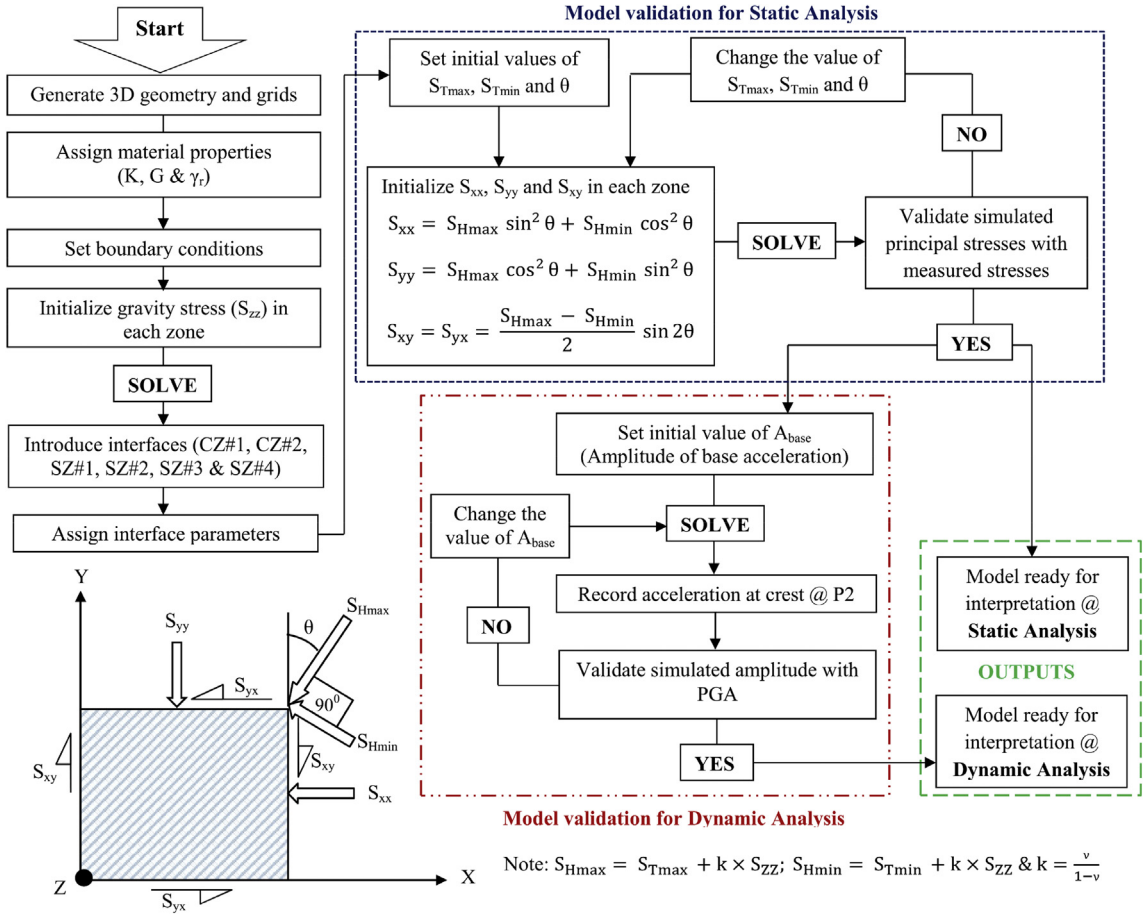

Fig. 9. Flowchart showing stress initialization, model validation and outputs for static and dynamic analyses in FLAC^{3D}.

shear stress initialized at the zones nearby the boundaries. However, the assumption here is that the overall model extent is fixed in such a way that the proximities of the boundaries do not influence the result at the area of interest. Since the boundaries are fixed, the stresses due to both gravity and tectonics are initialized in each element for whole geometry. However, the model is first initialized for gravity-induced vertical stress (S_{zz}) only in the homogeneous material before introducing the major weakness planes and the model is solved for the equilibrium state. The values of S_{zz} for each zone in the model are saved. This is particularly done to generate the vertical stress in each zone of the model almost equal to the theoretical vertical stress given by the overburden depth. The fact is that if the model is not homogeneous and the loading is not merely vertical stress, experience shows that the value of S_{zz} will be attenuated and will not be equal to the theoretical values. The interfaces representing the major weakness and shear zones (CZ#1, CZ#2, SZ#1, SZ#2, SZ#3 and SZ#4) are then introduced into the model and respective interface parameters are assigned.

The model validation process for static analysis is shown in Fig. 9. The magnitude and orientation of the maximum tectonic stress (S_{Tmax}) and the minimum tectonic stress (S_{Tmin}) are assumed first. The orientation of the maximum tectonic stress is denoted as θ. The total horizontal stress towards the tectonic stress directions for each zone is then calculated by adding the gravity-induced horizontal stress (which is calculated from the vertical stress extracted from the model) and the initially assumed tectonic stress magnitudes. The total horizontal stresses are resolved towards both x- and y-axis as normal stresses (S_{xx} and S_{yy}, respectively) and in xy-plane as shear stresses (S_{xy}) using the equations shown in Fig. 9. The total normal and shear stresses are further initialized in each zone for the whole geometry and the model is run for the equilibrium state once again. The process is repeated multiple times for various combinations of tectonic stress magnitudes and orientations until the simulated principal stresses converge to corresponding the principal stress magnitudes measured at the test tunnel. The output of the validated model is represented as 'Static Analysis'.

After the static analysis, a seismic acceleration is applied at the base of the same model as a dynamic loading. The seismic acceleration is applied in three directions, i.e. along north-south, east-west and vertical directions. An arbitrary value of the amplitude of the base acceleration is chosen as an initial value. The model is then run for the specified dynamic time period. The acceleration at a specified crest point is tracked during the simulation and the peak value is calculated, which is compared with the PGA at the same point. The amplitude of base acceleration is changed until the simulated peak acceleration at the surface becomes sufficiently closer to the PGA at the same surface location. Once the simulated value is close enough to the PGA, the model is said to be dynamically validated and the output in this case is represented as 'Dynamic Analysis', as shown in Fig. 9.

3.2. FLAC^{3D} model

Both static and dynamic analyses have been carried out using FLAC^{3D} software (Itasca, 2017). Geometry, material properties, and boundary and initial conditions are defined for the model extent generated in FLAC^{3D}. The Tamakoshi project area has a single rock formation (upper Himalayan crystalline) consisting of schistose

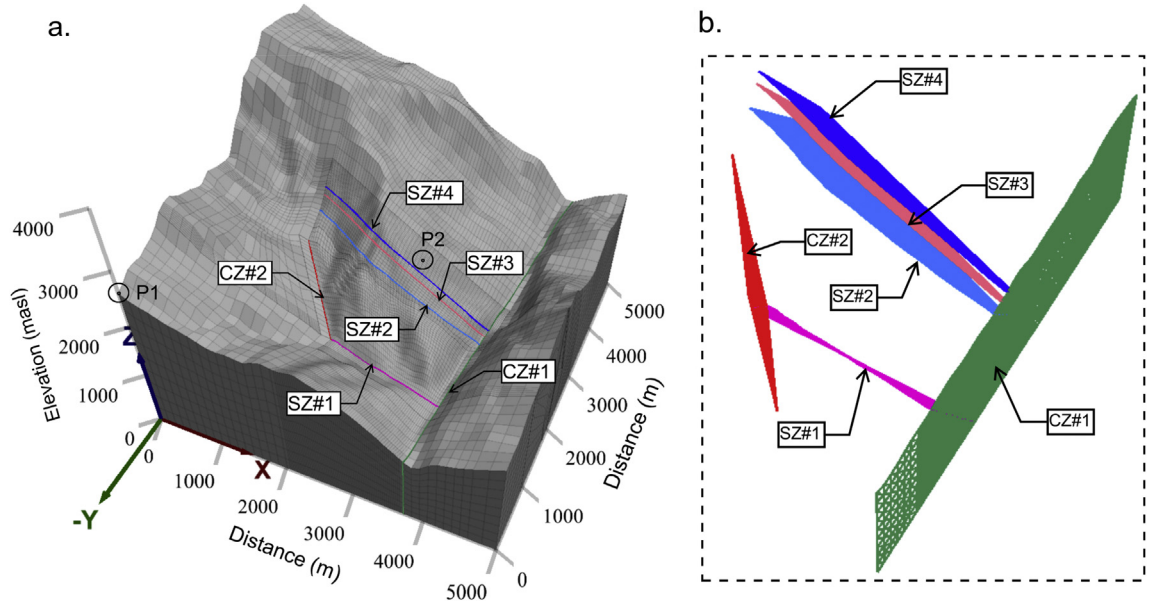

Fig. 10. (a) 3D geometry with terrain and (b) weakness zones.

gneiss where the homogeneity is disturbed by the major and minor shear and weakness zones (large-scale discontinuities), which are introduced in the model. Further, the rock mass is considered as an isotropic material even though the rock mass possess some degree of anisotropic behavior because of the developed schistosity. The constitutive equations derived for a linearly elastic model is used where the material is expected to exhibit linear stress–strain behavior. Principally, the adopted approach is correct for the in situ stress state evaluation of a large area as of UTHP and therefore the assumptions are representative enough to find the in situ stress state at UTHP.

3.2.1. Model geometry

As shown in Figs. 2a and 3a, the headrace tunnel along the old tunnel alignment becomes more critical as it approaches the downstream end. One of the reasons behind this is that the water pressure increases and reaches its maximum value of 420 m at the downstream end. In addition, there exist multiple topographic slopes towards both Gongar and Tamakoshi valleys at the downstream end of the headrace tunnel, which considerably influence the magnitude of in situ stresses at this outer part of the topography. Therefore, the most critical area of the headrace tunnel for the evaluation of stress state is considered to be beyond the headrace tunnel chainage 7 + 000 m towards the downstream end. The model extent (Fig. 2a) is thus chosen in such a way that the proximities of the model boundaries do not influence the area of interest. A 3D geometry is generated in FLAC^{3D} within the model extent (Fig. 10a). This geometry incorporates the topography shown in Fig. 2b. Positive *y*-axis of the geometry (Fig. 10a) is aligned towards the north. The size of the model along both *x*- and *y*-axis is 5000 m. The bottom of the model is at 0 masl and the depth of the model varies according to the topography inside the model extent. The major part of the geometry is meshed with finer brick-shaped elements in the area of interest and the size of the elements gradually becomes coarser towards the boundaries away from the area of interest. In addition, both wedge and tetrahedral shaped elements are used to fill the geometry in the rest of the irregular places. The meshes in the geometry are shown in Fig. 10a. In the model, a total of 641,124 3D elements are generated. The weakness and shear zones are also introduced in the model, as shown in Fig. 10a and b.

3.2.2. Input parameters to the model

The input parameters required for the model are quantified based on the detailed mapping, and information received from Tamakoshi project and laboratory testing. The parameters of rock mass and interface and tectonic stresses are the most important input variables to be quantified in carrying out the numerical analysis.

(1) Rock mass parameters

Rock mass parameters are required as inputs to define the quality of rock mass. Table 4 shows the mean values of rock mass parameters consisting of uniaxial compressive strength (UCS) of intact rock (σ_{ci}), Young's modulus of intact rock (E_i), Poisson's ratio (ν) and density of rock (ρ_r) and their respective SD. The mean values of the parameters shown in Table 4 are calculated from the results of laboratory tests carried out by Norconsult and Lahmeyer (2008) and SINTEF (2008). The bulk modulus (K) and shear modulus (G) of the intact rock in Table 4 are calculated following the equations suggested by Goodman (1989) for isotropic rock material.

Table 4
Mechanical properties of schistose gneiss and input parameters to FLAC^{3D}.

Density, ρ_r (kg/m^3)[a]		Poisson's ratio, ν[a]		Intact rock strength (UCS), σ_{ci}[a] (MPa)		Young's modulus, E_i[a] (GPa)		Bulk modulus, K (GPa)[b]		Shear modulus, G (GPa)[c]	
Mean	SD	Mean	SD	Mean	SD	Mean	SD	Mean	SD	Mean	SD
2745	26	0.2	0.1	61	18	30.2	7.9	16.8	5.5	12.6	4

[a] The values of the parameters are calculated from laboratory test results.
[b] $K = E_i/[3(1-2\nu)]$.
[c] $G = E_i/[2(1+\nu)]$.

(2) Interface parameters

In FLAC^{3D}, all six shear and crushed zones are modeled as interfaces. The interface parameters such as stiffness and friction angle are important in numerical simulation using FLAC^{3D} (Itasca, 2017). Rock mass stiffness of the weakness and shear zones depends on the elasticity properties of the zones such as Young's modulus (E_0), shear modulus (G_0) and thickness of the zone (w_t). Both normal stress (S_n) and shear stress (S_s) are acting on the weakness zone, as indicated in Fig. 11. According to Li et al. (2009), the normal stiffness (k_n) and shear stiffness (k_s) of the weakness and shear zones can be estimated if the values of E_0, G_0 and w_t are known (Fig. 11).

The Young's modulus of the material at the weakness zone is assumed equal to the deformation modulus of the rock mass at that zone based on the explanations given by Hoek et al. (1998) and Marinos (2010). This assumption is made due to the lack of laboratory tested Young's modulus of the rock material from the rock mass in the weakness zone of UTHP since no core recovery having length longer than 1.5 times the diameter of the core was achieved while drilling through the weakness zones. The relationship given by Hoek and Diederichs (2006) is used to calculate the deformation modulus of the weakness zone material. Hoek and Diederichs (2006) used *GSI* value, modulus of elasticity and disturbance factor (D) in their relationship. During excavation of the headrace tunnel of the UTHP, the *Q*-values (Barton et al., 1974) are mapped along the tunnel alignment. First, the relationship suggested by Barton (1995) is used to estimate the *RMR* values from the mapped *Q*-values at the shear zones and then the *GSI* values are calculated using the equation proposed by Hoek and Diederichs (2006). Average *Q*-value of most of the weakness and shear zones mapped along the headrace and tailrace tunnels is approximately 0.05, which gives *GSI* value of approximately 25. Hence, *GSI* value of 25 is considered as a representative value for all weakness and shear zones in the UTHP area. The estimated and calculated interface parameters are shown in Table 5, where ν_0 is the Poisson's ratio of the weakness zone material, which is taken as 0.1 based on Panthi (2006).

Friction angle of the interface is also an important parameter to be estimated for the simulation. Usually, it ranges from 15° to 30° in case of faults and weakness zones (Barton, 1973). Friction angle of 25° is estimated as the most likely value based on the observation and rock mass quality description of the weakness and shear zones encountered at the tailrace and headrace tunnels. The estimated interface parameters are given in Table 5.

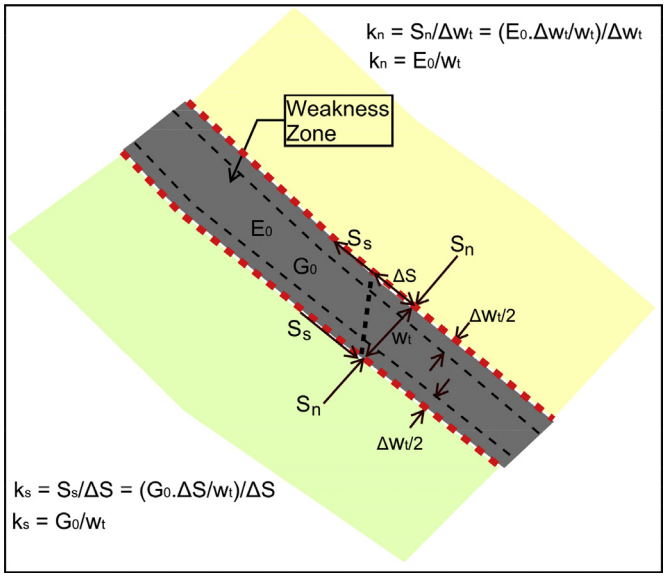

Fig. 11. Weakness zone in between the relatively stiff rock masses.

3.2.3. Stresses

Stress is another key parameter in numerical simulations. The stress along the *z*-axis (S_{zz}) is mainly due to the vertical overburden (h) of the rock mass. Part of the horizontal stress is due to the vertical overburden, which is related to the Poisson's ratio. In FLAC^{3D}, *y*-axis is aligned to the north direction. The normal stresses along the *x*- and *y*-axis and corresponding shear stresses are calculated by resolving the total maximum horizontal stress (S_{Hmax}) and total minimum horizontal stress (S_{Hmin}), as shown in Fig. 9. The total maximum and minimum horizontal stresses are calculated by adding the horizontal stress induced by the vertical overburden and respective maximum tectonic stress (S_{Tmax}) and minimum tectonic stress (S_{Tmin}), respectively. The total stresses along the *x*- and *y*-axis are calculated using the equations given in Fig. 9. Since the maximum horizontal stress makes an angle (θ) with *y*-axis, there will be shear stresses in *yz* and *xz* planes, as indicated in Fig. 9 (the box shown in the figure has thickness along *z*-axis). The shear stresses will have the same magnitude in both planes and are estimated using the equation shown in Fig. 9, which are negative in FLAC^{3D}.

3.2.4. Seismic acceleration at the base of the model

In FLAC^{3D}, the acceleration is applied at the base of the model. It is highlighted here that the PGA values represent the worst case scenario that gives the maximum change in the stress values, which are of primary interest in this study. Certainly, historical data would have enhanced the accuracy of the analysis, but due to the lack of availability of historically recorded data, no time history was possible to be used in the model. Therefore, for simplicity, the seismic acceleration at the base is considered to have the characteristics of sinusoidal wave. The base acceleration (a_{base}) at time t can then be expressed as (Itasca, 2017):

$$a_{base} = E_f A_{base} \sin(2\pi f t) \tag{2}$$

$$E_f = \frac{1}{2}\left[1 - \cos\left(\frac{2\pi}{T}t\right)\right] \tag{3}$$

where T is the total duration of the wave, f is the frequency of the wave, A_{base} is the amplitude of the wave, and E_f is an envelope function. The envelope function provides a gradual built-up and decay of the wave over the total duration of the wave. In the UTHP, the characteristics of the base acceleration are considered as that recorded in the seismic stations at Kathmandu for the aftershock of $M_w = 7.3$. According to Bhattarai et al. (2015), the corresponding frequency of seismic wave is about 1 Hz, which is estimated by taking the reference from the seismic wave characteristics measured at different seismological stations at Kathmandu, Nepal.

3.3. Model validation

3.3.1. Static analysis

For the validation purpose, the model is run for different tectonic stress magnitudes and orientations so that the output results are comparable with measured stresses at respective locations. In doing so, the model is first run multiple times in order to find the possible ranges of tectonic stress magnitudes and directions, respectively. Possible ranges of tectonic stresses are decided with

Table 5
Input parameters for interfaces.

Interfaces	E_i (GPa)	Q	GSI	E_0 (GPa)	ν_0	G_0 (GPa)	w_t (m)	k_n (Pa/m)	k_s (Pa/m)	Friction angle (°)
CZ#1	30.2	0.05	25	1.8	0.1	0.82	35	5.1×10^7	2.3×10^7	25
CZ#2	30.2	0.05	25	1.8	0.1	0.82	25	7.2×10^7	3.3×10^7	25
SZ#1	30.2	0.05	25	1.8	0.1	0.82	25	7.2×10^7	3.3×10^7	25
SZ#2	30.2	0.05	25	1.8	0.1	0.82	30	6×10^7	2.7×10^7	25
SZ#3	30.2	0.05	25	1.8	0.1	0.82	35	5.1×10^7	2.3×10^7	25
SZ#4	30.2	0.05	25	1.8	0.1	0.82	15	1.2×10^8	5.5×10^7	25

Note: $GSI = RMR - 5$, $RMR = 15\log_{10}Q + 50$, $E_0 = E_i\{0.02 + (1 - D/2)/[1 + e^{(60+15D-GSI)/11}]\}$, $G_0 = E_0/[2(1 + \nu_0)]$, $k_n = E_0/t$, and $k_s = G_0/t$.

the help of the magnitude and orientation of the measured stresses at the test tunnel and the orientation of the maximum tectonic stress regime of the area as recommended by Panthi (2012). The model is validated within the possible ranges of S_{Tmax} from 15 MPa to 25 MPa, θ from N20°E to N40°E, and S_{Tmin} from 0 to 10 MPa. The model is then run for all possible combinations of tectonic stress magnitudes and orientations (see Table 6). The simulated principal stresses from the model are compared with those at different test locations. The orientations of the principal stresses from the model are also compared with corresponding orientations measured at test tunnel. The best possible simulation has been achieved when the maximum tectonic stress of about 20 MPa is acting in the orientation of N25°E and the corresponding minimum tectonic stress is about 5 MPa (trial No. 28 in Table 6). The magnitudes of simulated principal stresses in this case are plotted in Fig. 12 where the mean values of measured principal stresses with SDs at all test locations are also plotted. In addition, the orientations of both simulated and measured principal stresses at test tunnel for the best case are also plotted in the stereographic projection (Fig. 13). It is highlighted that the simulated orientation of S_1 is closer to the measured orientation in location TT2 and the simulated orientations of S_2 and S_3 are closer to the measured ones in locations TT2 and TT3. After some more attempts, it is realized that matching both magnitude and orientation of simulated stresses with that of the measured stresses at all locations is almost impossible since both magnitude and orientation are attenuated due to local geological features. However, the best case has been achieved considering magnitudes as well as orientations. More importantly, Fig. 12 shows that eleven out of thirteen simulated results are within one SD of the mean values of the measured stresses, which represents about 85% of the total measurements. Considering this result, the model is assumed to be validated satisfactorily.

3.3.2. Dynamic analysis

Once the model is validated statically, dynamic analysis is carried out by applying the seismic acceleration as dynamic input at the base of the model in FLAC^{3D}. During simulation, the surface acceleration is tracked at location P2 (as shown in Fig. 10) over the whole dynamic time period of 60 s. The maximum amplitude of the simulated acceleration at P2 is calculated by plotting the acceleration over the specified dynamic time period. The maximum acceleration is then considered as the simulated PGA at location P2 and is compared with the estimated PGA of 0.4g as shown in Fig. 8. The amplitude of the base acceleration is changed until the simulated PGA at P2 becomes closer to the PGA value of about 0.4g (4 m/s^2). The simulated PGA at P2 reaches close to 0.4g for the amplitude of base acceleration (A_{base}) of about 1.2 m/s^2 with corresponding frequency of the base acceleration of 1 Hz. This stage of simulation is considered to be validated dynamically. The total duration of base acceleration is 18 s, which accelerates the surface to about 30 s. Both the crest and base accelerations from the validated model during the dynamic time period are shown in Fig. 14.

4. Results and discussion

As expected, the simulation results have indicated that there is a significant influence of tectonic stress on the overall stress state in the Tamakoshi area. The model is validated for the maximum tectonic stress of 20 MPa with an orientation of N25°E. The corresponding minimum tectonic stress is about 5 MPa. After validation, the magnitude of the minimum principal stress is extracted from the model for further assessment on the applicability of shotcrete lined pressure tunnel. Fig. 15 shows the magnitude of the minimum principal stress at vertical sections cut along both OLD HRT (Fig. 15a) and NEW HRT (Fig. 15b). The minimum principal stress in the figure is output from the static analysis.

Fig. 15 indicates that the stress magnitude is attenuated due to the presence of the Gongar valley, which also is the shear zone (SZ#1). As one can see in the figure, there is considerable stress attenuation due to the presence of local shear zones at the tunnel alignments.

Further, the magnitude of the minimum principal stresses is extracted from the model results of static and dynamic analyses so that an overview of their magnitude is statistically assessed with respect to the static water head (P_w) acting along the tunnel alignment (Fig. 16). The static water head shown in the figure is the

Table 6
Different combinations of tectonic stress magnitudes and orientations.

Trial No.	S_{Tmax} (MPa)	S_{Tmin} (MPa)	θ (°)	Trial No.	S_{Tmax} (MPa)	S_{Tmin} (MPa)	θ (°)	Trial No.	S_{Tmax} (MPa)	S_{Tmin} (MPa)	θ (°)
1	15	0	20	14	20	5	30	27	25	10	40
2	15	0	30	15	20	5	40	28	20	5	25
3	15	0	40	16	20	10	20	29	20	5	35
4	15	5	20	17	20	10	30	30	20	5	23
5	15	5	30	18	20	10	40	31	20	5	27
6	15	5	40	19	25	0	20	32	20	5	26
7	15	10	20	20	25	0	30	33	20	5	24
8	15	10	30	21	25	0	40	34	20	4	25
9	15	10	40	22	25	5	20	35	20	6	25
10	20	0	20	23	25	5	30	36	18	5	25
11	20	0	30	24	25	5	40	37	21	5	25
12	20	0	40	25	25	10	20	38	19	5	25
13	20	5	20	26	25	10	30				

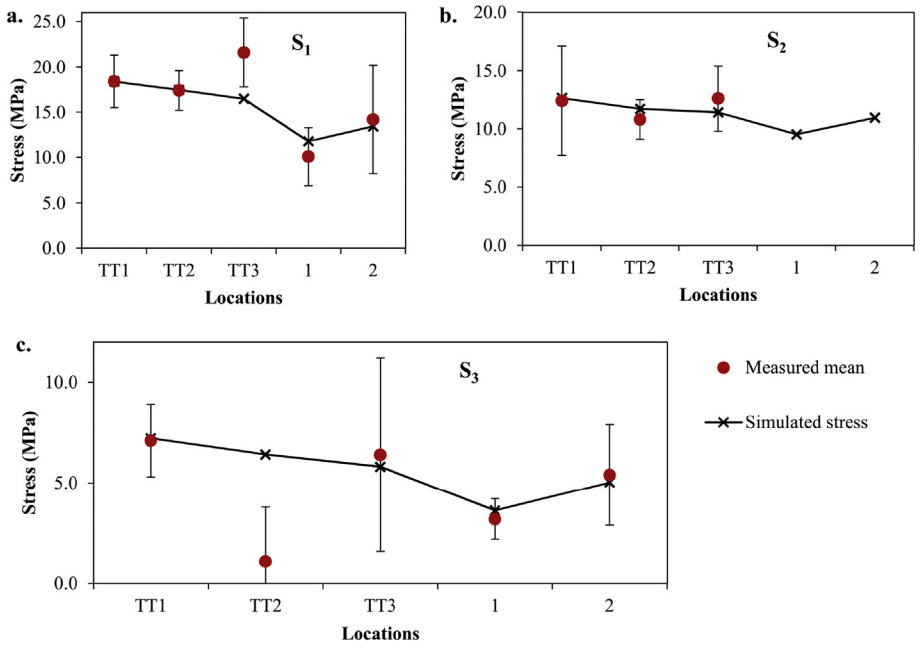

Fig. 12. The measured and simulated principal stresses: (a) Maximum principal stress (S_1); (b) Intermediate principal stress (S_2); and (c) The minimum principal stress (S_3).

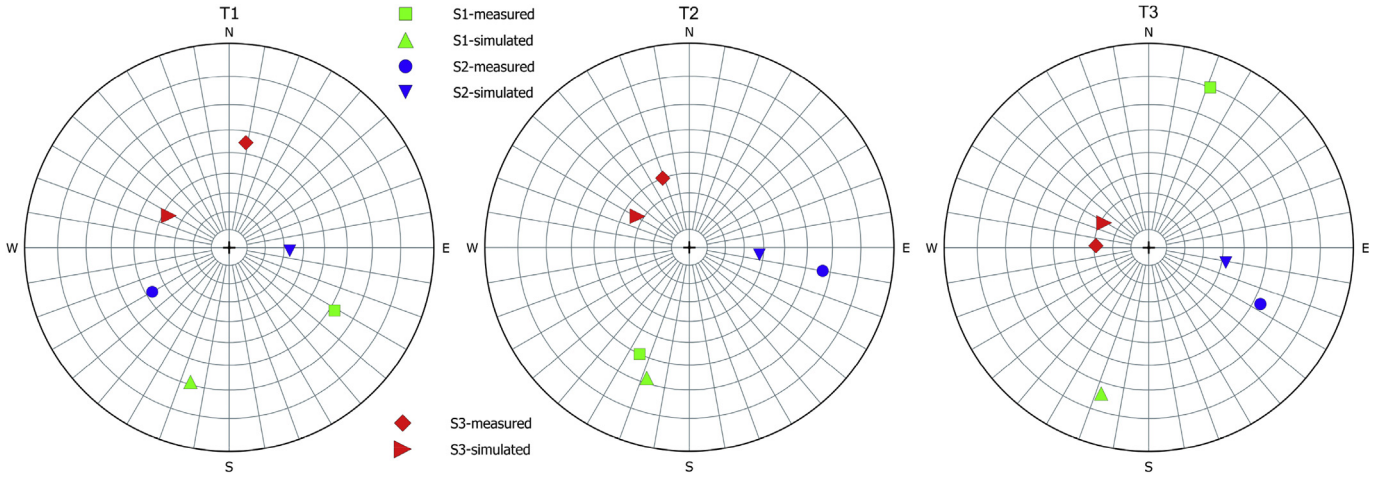

Fig. 13. Stereo-plot (equal angle projection; lower hemisphere) of orientation of both simulated and measured principal stresses at locations TT1, TT2 and TT3 for trial No. 28 (i.e. $S_{Tmax} = 20$ MPa, $S_{Tmin} = 5$ MPa, and $\theta = 25°$). The results from Basnet and Panthi (2018) are slightly updated.

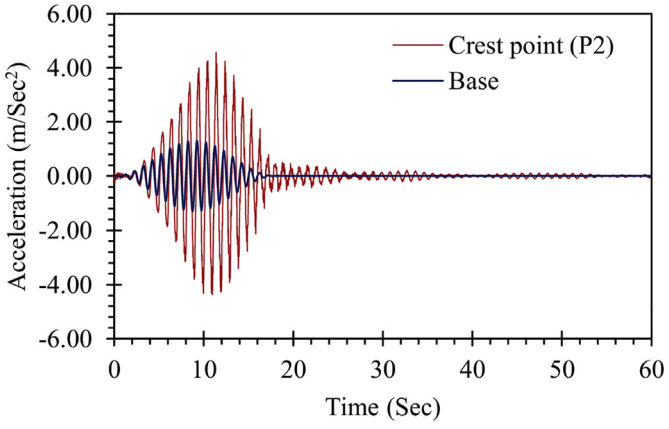

Fig. 14. The seismic accelerations at base and crest of the given 3D model.

vertical height difference between the highest water level (HWL), which is 1987 masl in Fig. 3a, and the location of the shotcrete lined pressure tunnel. Both the minimum principal stress magnitudes and water pressure are plotted for both OLD HRT (Fig. 16a) and NEW HRT (Fig. 16b) alignments. As one can see in Fig. 16, the magnitude of the minimum principal stress is less than the water pressure at tunnel locations where shear zones are presented. The simulation results indicate that the minimum principal stress magnitudes are considerably lower than the static water pressure acting on the headrace tunnel, which indicates that there is a high risk of hydraulic jacking, especially at and nearby the areas where shear zones are located. In addition, one can see that at each dynamic (seismic) loading, there is risk of reduction in the minimum principal stress magnitudes at the areas where shear zones are located, which is mainly due to destressing effect during dynamic seismic loading.

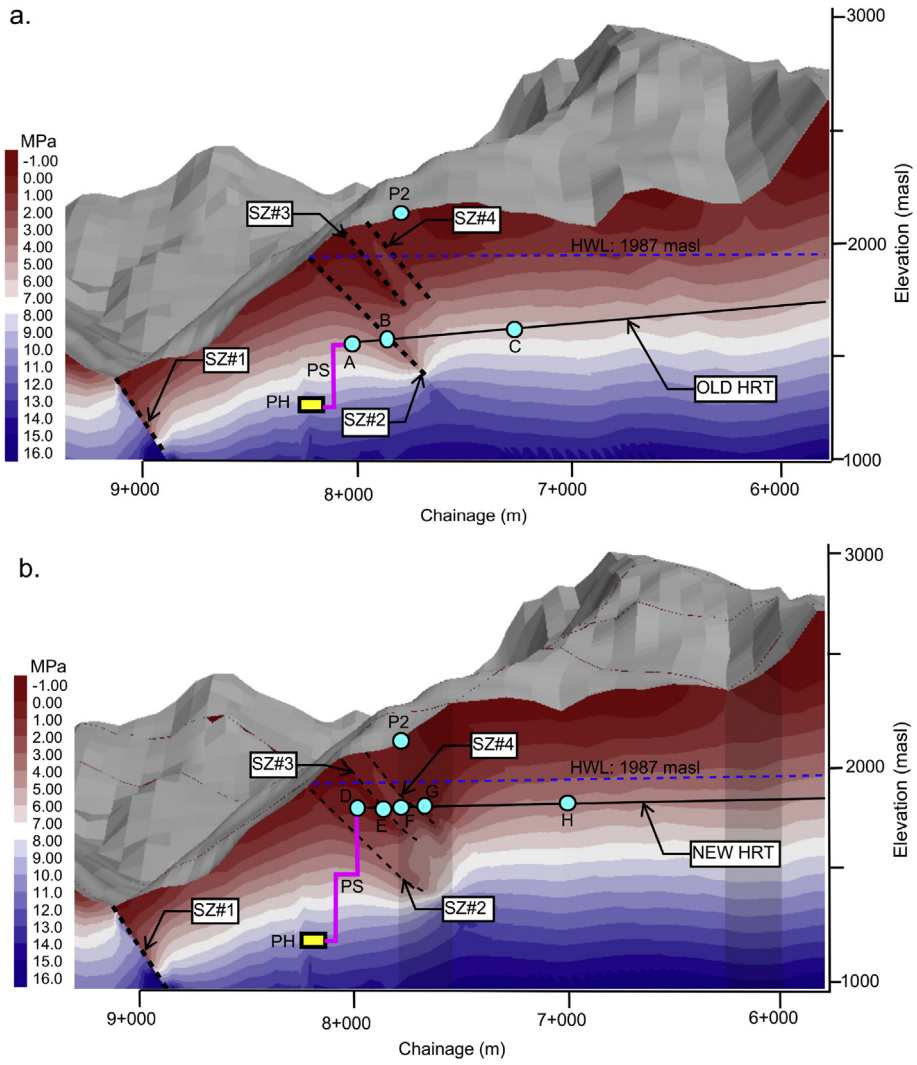

Fig. 15. The minimum principal stress (MPa) after static analysis along (a) OLD HRT (*y*-*y*) and (b) NEW HRT.

Besides, the stress reduction at the downstream locations can also be inferred to the situation that the confinement from both Gongar and Tamakoshi valley sides decreases as we go further out towards Gongar valley. The ground shaking due to earthquake has considerable impact on the rock mass located at the high relief area with lower lateral confinement caused by steep topography like that at the outer reach of the headrace tunnel of the UTHP. Similar is the case beyond SZ#3 towards the downstream end of the NEW HRT (Fig. 16b). However, it is noted here that the minimum principal stress magnitudes in locations upstream from SZ#2 at OLD HRT and from SZ#4 at NEW HRT are not affected by the dynamic loading. This indicates that if the rock mass is strong, homogeneous and of good quality, the risk of destressing effect is minimum, and even in some occasion, the stresses may be accumulated.

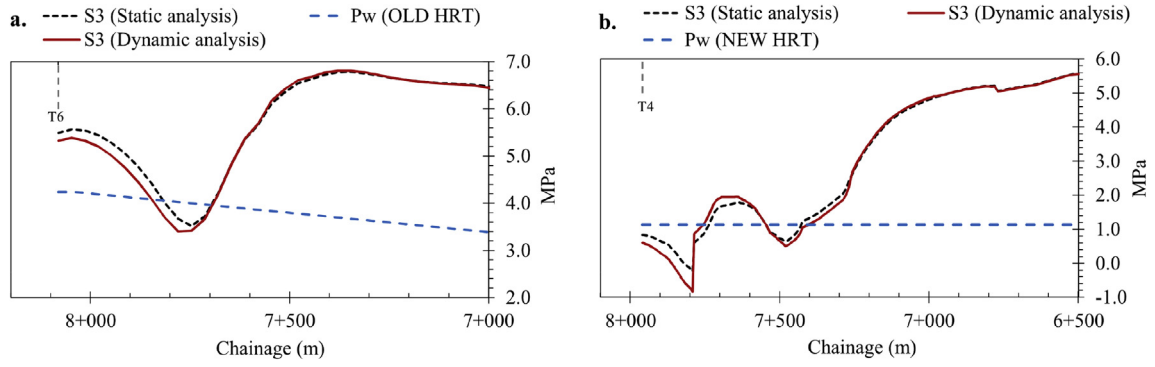

Fig. 16. The minimum principal stress (both static and dynamic analyses) and static water pressure (P_w) at tunnel location along (a) OLD HRT and (b) NEW HRT.

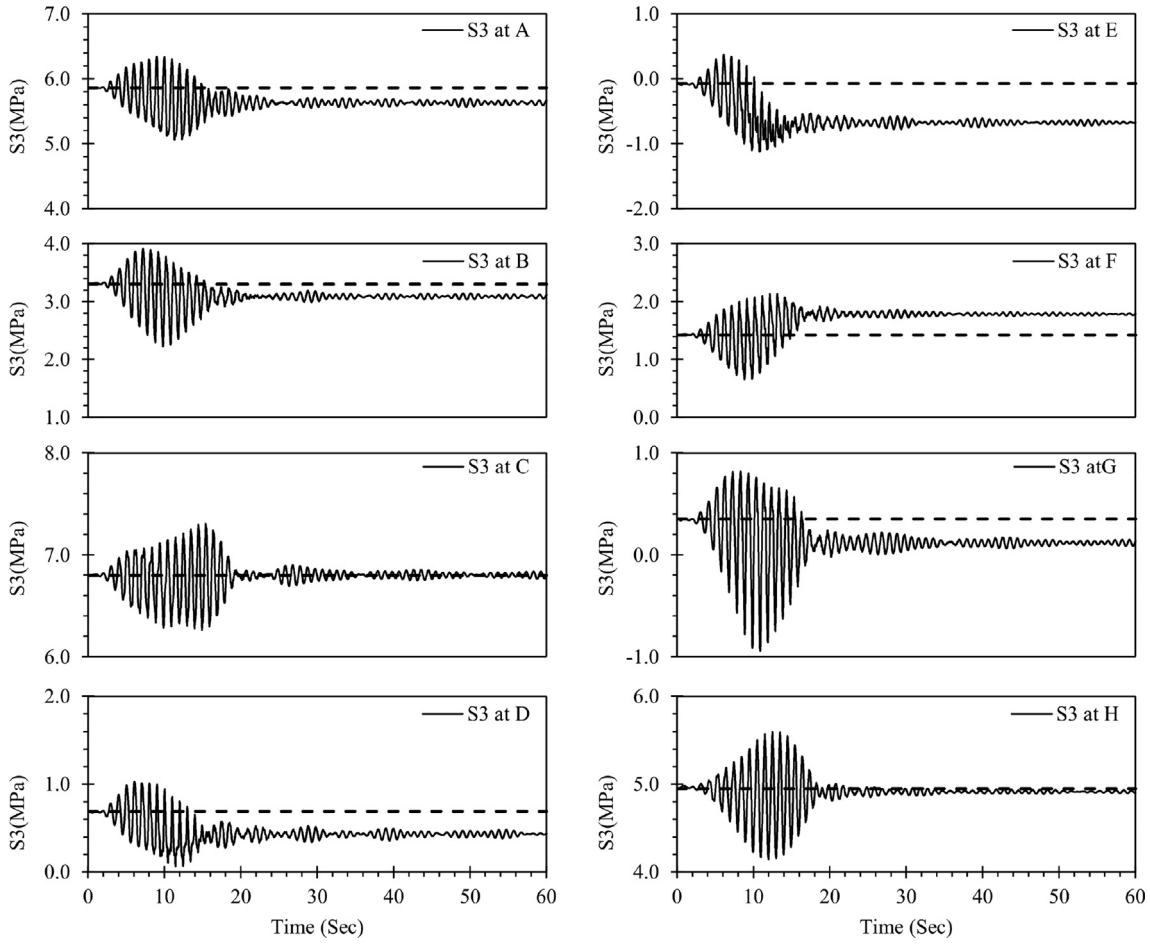

Fig. 17. The minimum principal stress recorded over the dynamic time period in 3D model at locations A, B and C along OLD HRT and D, E, F, G and H along NEW HRT.

Likewise, an attempt is also made to assess the pattern of changes in the magnitude of the minimum principal stress during the whole shaking period of 60 s at the selected locations represented as A, B, C, D, E, F, G and H marked in Fig. 15. The change patterns in the magnitude of the minimum principal stress during dynamic loading period (shaking period) at each of the selected locations (i.e. A, B and C at OLD HRT, and D, E, F, G and H at NEW HRT alignment) are shown in Fig. 17. Fig. 17 indicates that there is considerable fluctuation in the stress magnitude during the peak of acceleration and it stabilizes once the peak acceleration dies out. The magnitudes of the minimum principal stress at locations C and H eventually dampen and reach their original values, which belong to the points where intact rock mass exists and is far from the shear zones. On the other hand, at locations B, E and G where shear zones are located, the minimum principal stresses are stabilized to a new stress magnitude, which is lower than the original one. This indicates that the weakness and fault zones are vulnerable areas during seismic events and permanent changes in the in situ stress state are eminent. In addition, as one can see in Fig. 17, the magnitudes of the minimum principal stress have also changed at locations A, D and F that are located nearby the shear zones. The stress magnitudes at the locations A and D are slightly reduced after the shaking period. In contrast, the stress magnitude at location F is increased after the earthquake event indicating that there is an accumulation of stress between the two shear zones, which is quite logical.

5. Conclusions

The static simulation carried out to assess the magnitude of the in situ minimum principal stress suggests that the stress state at the outer reach of shotcrete lined headrace tunnel at UTHP is very much influenced by the slope topography of two valleys and the presence of weakness and shear zones. The 3D topography and the presence of weakness and shear zones in the area are the major issues that need to be extensively evaluated before selecting shotcrete lined high pressure headrace tunnel system. As demonstrated in this paper, the downstream end of the headrace tunnel at both old and new tunnel alignments of the Tamakoshi project has the likelihood that hydraulic jacking and leakage may occur during the operation of the plant. The dynamic seismic simulation further indicates that there is permanent reduction in the stress state at areas where weakness and shear zones are located, suggesting that there is even increased risk of hydraulic jacking and excessive leakage. This analysis signifies that the dynamic analysis in addition to the static analysis should be carried out to assess the in situ stress state in a seismically active region like in the Himalaya.

Conflicts of interest

The authors wish to confirm that there are no known conflicts of interest associated with this publication and there has been no

significant financial support for this work that could have influenced its outcome.

References

Basnet CB, Panthi KK. Evaluation of in situ stress state along the shotcrete lined high-pressure headrace tunnel at a complex Himalayan geological condition. Geosystem Engineering 2018. https://doi.org/10.1080/12269328.2018. 1548306.

Barton N. A review of the shear strength of filled discontinuities in rock. In: Fjellspregningsteknikk, Bergmekanikk. Trondheim, Norway: Tapir Press; 1973. p. 19.1–19.38.

Barton N, Line R, Lunde J. Engineering classification of rock masses for the design of tunnel support. Rock Mechanics 1974;6(4):189–236.

Barton N. The influence of joint properties in modelling jointed rock masses. In: 8th ISRM congress. A.A. Balkema; 1995. p. 1023–32.

Bergh-Christensen J. Design of unlined pressure shaft at Mauranger power plant, Norway. In: ISRM international symposium. A.A. Balkema; 1982.

Bhattarai M, Adhikari LB, Gautam UP, Laurendeau A, Labonne C, Hoste-Colomer R, Sebe O, Hernandez B. Overview of the large 25 April 2015 Gorkha, Nepal, earthquake from accelerometric perspectives. Seismological Research Letters 2015;86(6):1540–8.

Bird P. Initiation of intracontinental subduction in the Himalaya. Journal of Geophysical Research: Solid Earth 1978;83(B10):4975–87.

Broch E. The development of unlined pressure shafts and tunnels in Norway. In: ISRM international symposium. A.A. Balkema; 1982.

Buen B, Palmstrom A. Design and supervision of unlined hydro power shafts and tunnels with head up to 590 meters. In: ISRM international symposium. A.A. Balkema; 1982.

Buen B. Documentation unlined water conduits in Norway. In: Hard rock engineering. Oslo, Norway: FHS; 1984.

Goodman RE. Introduction to rock mechanics. 2nd ed. New York: Wiley; 1989.

Haimson BC, Cornet FH. ISRM suggested methods for rock stress estimation – part 3: hydraulic fracturing (HF) and/or hydraulic testing of pre-existing fractures (HTPF). International Journal of Rock Mechanics and Mining Sciences 2003;40(7–8):1011–20.

Hart R. Enhancing rock stress understanding through numerical analysis. International Journal of Rock Mechanics and Mining Sciences 2003;40(7–8):1089–97.

Hoek E, Marinos P, Benissi M. Applicability of the geological strength index (GSI) classification for very weak and sheared rock masses. The case of the Athens Schist Formation. Bulletin of Engineering Geology and the Environment 1998;57(2):151–60.

Hoek E, Diederichs MS. Empirical estimation of rock mass modulus. International Journal of Rock Mechanics and Mining Sciences 2006;43(2):203–15.

Hudson JA, Cornet FH, Christiansson R. ISRM suggested methods for rock stress estimation – part 1: strategy for rock stress estimation. International Journal of Rock Mechanics and Mining Sciences 2003;40(7–8):991–8.

International Society for Rock Mechanics (ISRM). Suggested method for determining indirect tensile strength by the Brazil test. International Journal of Rock Mechanics and Mining Sciences & Geomechanics Abstracts 1978;15(3):102–3.

Itasca. FLAC^{3D} 6.0 user's manual. Minneapolis, USA: Itasca Consulting Group; 2017.

Li G, Mizuta Y, Ishida T, Li H, Nakama S, Sato T. Stress field determination from local stress measurements by numerical modelling. International Journal of Rock Mechanics and Mining Sciences 2009;46(1):138–47.

Lu M. Interpretation of in-situ rock stress measurement by overcoring. In: Lu M, Li CC, editors. In-situ rock stress: measurement, interpretation and application, proceedings of the international symposium on in-situ rock stress. London: Taylor & Francis; 2006. p. 393–8.

Marinos PV. New proposed GSI classification charts for weak or complex rock masses. Bulletin of the Geological Society of Greece 2010;43(3):1248–58.

McGarr A, Gay NC. State of stress in the Earth's crust. Annual Review of Earth and Planetary Sciences 1978;6(1):405–36.

Nakata T, Otsuki K, Khan SH. Active faults, stress field and plate motion along the Indo-Eurasian plate boundary. Tectonophysics 1990;181(1–4):83–8. 91–95.

Norconsult. Feasibility study report of upper Tamakoshi hydroelectric project, Nepal. Sandvika, Norway: Norconsult; 2005.

Norconsult, Lahmeyer. Detailed design report of upper Tamakoshi hydroelectric project. Nepal: Norconsult and Lahmeyer; 2008.

Panthi KK. Analysis of engineering geological uncertainties related to tunnelling in Himalayan rock mass conditions. PhD Thesis. Trondheim, Norway: Norwegian University of Science and Technology; 2006.

Panthi K. Evaluation of rock bursting phenomena in a tunnel in the Himalayas. Bulletin of Engineering Geology and the Environment 2012;71(4):761–9.

Panthi KK. Norwegian design principle for high pressure tunnels and shafts: its applicability in the Himalaya. Hydro Nepal. Journal of Water, Energy and Environment 2014;(14):36–40.

Panthi KK, Basnet CB. Design review of the headrace system for the Upper Tamakoshi project, Nepal. International Journal on Hydropower and Dams 2017;24(1):60–7.

Reimer W, Bock H. Report on the October 2013 project mission, upper Tamakoshi Hydroelectric project. Members of the panel of experts for the project; 2013.

SINTEF. Rock stress measurement at the upper Tamakoshi Hydroelectric project. SBF IN F08112. Trondheim, Norway: SINTEF; 2008.

SINTEF. Rock stress measurement by hydraulic fracturing at the Upper Tamakoshi Hydroelectric project, Nepal. SBF IN F08112. Trondheim, Norway: SINTEF; 2013.

Selmer-Olsen R. Experience with unlined pressure shafts in Norway. In: Brekke TL, Jörstad FA, editors. Proceedings of international symposium on large permanent underground openings. Oslo, Norway: Universitetsforlaget; 1969.

Selmer-Olsen R. Underground openings filled with high-pressure water or air. Bulletin of the International Association of Engineering Geology 1974;9(1):91–5.

U.S. Geological Survey (USGS). ShakeMap of *M* 7.3 aftershock – 19 km SE of Kodari, Nepal. Reston, USA: USGS; 2015. https://earthquake.usgs.gov/earthquakes/eventpage/us20002ejl#shakemap.

Krishna Kanta Panthi is Professor in Geological Engineering at the Department of Geoscience and Petroleum, Norwegian University of Science and Technology (NTNU), Trondheim, Norway. He holds the degrees of PhD (Dr.Ing.) in Rock Engineering, MSc in Hydropower Development and MSc in Tunneling. He has over 27 years of experience in research, design and implementation of rock engineering, tunneling, hydropower, mining and slope engineering projects. He is the author of over 70 scientific articles and book chapters published in internationally recognized journals and conference proceedings.

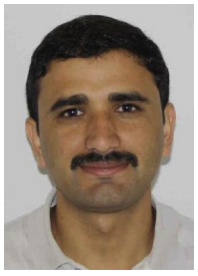

Chhatra Bahadur Basnet is a rock engineering expert who works at the NEA Engineering, Kathmandu, Nepal since January 2019. He has completed his MSc degree in Hydropower Development in 2013 and PhD degree in Rock Engineering in late 2018 from the NTNU, Norway. He has over 8 years of experience in research, design and implementation of hydropower projects in the Himalayan geological conditions. He is the author of many scientific papers published in internationally recognized journals and conference proceedings.